

## Multiparticle production on hydrogen, argon, and xenon targets in a streamer chamber by 200-GeV/c proton and antiproton beams

C. De Marzo, M. De Palma, A. Distanto, C. Favuzzi, G. Germinario, P. Lavopa, G. Maggi, F. Posa, A. Ranieri, G. Selvaggi, P. Spinelli, and F. Waldner  
*Istituto di Fisica dell'Università di Bari and Istituto Nazionale di Fisica Nucleare, Bari, Italy*

A. Białas, W. Czyż, A. Eskreys, K. Eskreys, K. Fialkowski, D. Kisielewska, B. Madeyski, P. Malecki, K. Olkiewicz, and B. Pawlik  
*Institute of Nuclear Physics, Institute of Physics and Nuclear Techniques of Academy of Mining and Metallurgy, and Jagellonian University, Krakow, Poland*

W. H. Evans,<sup>‡</sup> J. R. Fry, C. Grant, M. Houlden, A. Morton, H. Muirhead, J. Shiers, and S. L. Wong  
*University of Liverpool, Liverpool, United Kingdom*

M. Antic,\* W. Baker,<sup>†</sup> T. Coghren,<sup>§</sup> F. Dengler, I. Derado, V. Eckardt, J. Fent, P. Freund, H. J. Gebauer, T. Kahl, R. Kalbach,<sup>‡</sup> A. Manz, P. Polakos, K. P. Pretzl, N. Schmitz, T. Schouter P. Seyboth, J. Seyerlein, P. Stopa,<sup>§</sup> D. Vranic,\* and G. Wolf  
*Max-Planck-Institut für Physik und Astrophysik, München, Germany*

F. Crijs, W. J. Metzger, C. Pols, and T. Spuijbroek  
*University of Nijmegen and NIKHEF, Nijmegen, Netherlands*  
(Received 8 March 1982)

Interactions of 200-GeV/c protons and antiprotons on hydrogen, argon, and xenon targets were studied with a streamer-chamber vertex spectrometer at the CERN SPS. Results on multiplicities, rapidity distributions, and correlations are presented and compared with predictions of current models.

### I. INTRODUCTION

In recent years there have been a large number of papers, both experimental and theoretical, on various aspects of high-energy collisions with nuclei.<sup>1</sup> In such collisions one can investigate the space-time development of the formation of produced hadrons as the nucleons in the nucleus serve as detectors for the products of the initial interaction. In particular, naive expectations assuming instantaneous particle production are not confirmed by the data, as, e.g., the average produced particle multiplicity is much smaller than expected from intranuclear cascading. This observation leads to the construction of models in which hadron formation occurs outside the nucleus and no cascading is present. However, the abundance of relatively slow secondaries shows that cascading cannot be neglected. It is important to find the range of momenta for which cascading occurs since it puts constraints on the models which may change their predictions also in other regions of phase space. The experimental data are not yet detailed enough

to differentiate between the various models. In contrast to existing data on heavy nuclei, this experiment determined the momenta and charges of all charged particles in the final state, for both nuclear and elementary targets. Furthermore slow protons were identified, the number of which gives an estimate of the number of interactions inside the nucleus.<sup>2</sup>

In this paper we present results on particle production in collisions of 200-GeV/c protons and antiprotons with hydrogen, argon, and xenon targets. The experiment uses a streamer-chamber vertex spectrometer with a  $4\pi$  solid-angle coverage, excellent multitrack efficiency, and the ability to identify slow particles by ionization. Some preliminary results have been reported elsewhere.<sup>3</sup> The organization of the paper is as follows: The experimental apparatus and the trigger are described in Sec. II, the data-analysis procedure is described in Sec. III, and the experimental results are presented and discussed in Sec. IV and compared to some predictions of current models in Sec. V. A summary and conclusions are contained in Sec. VI.

## II. EXPERIMENTAL APPARATUS AND TRIGGER

The experiment was performed at the CERN SPS using the unseparated H<sub>2</sub> beam at 200 GeV. Protons and antiprotons were tagged by differential Cherenkov counters. The beam rate was up to  $10^5$  particles per second.

The apparatus is shown schematically in Fig. 1. It consists of a streamer chamber inside a superconducting vertex magnet, seven large magnetostrictive spark chambers, four small proportional chambers (PC's) and beam-defining counters. The streamer chamber with dimensions  $2 \times 1.4 \times 0.72$  m<sup>3</sup> had three gaps (0.18 m, 0.36 m, 0.18 m) in order to avoid an electrode near the beam region.<sup>4</sup> It was filled with a helium-neon gas mixture at atmospheric pressure and was operated with high-voltage pulses of  $\pm 350$  kV and 12-nsec duration. The memory time was reduced to  $\sim 2$   $\mu$ sec by adding 0.1 ppm of the electronegative gas SF<sub>6</sub> to the helium-neon mixture in order to operate in a beam of the quoted intensity. The streamer chamber was photographed by three cameras fitted with single-stage electrostatic image intensifiers (type VARO 8605) at a demagnification of 60. The setting error in space was 0.4 mm. The chamber was inside a superconducting magnet giving a 1.5-T field. Figure 2 shows a photograph of a proton-xenon interaction producing about 60 charged particles.

The downstream spectrometer consisted of seven magnetostrictive spark chambers which were used to improve the momentum measurement. In the beam region three additional small multiwire proportional chambers served to identify accidental beam particles. The measuring accuracy was  $\Delta p/p = 0.0025p$  ( $p$  in GeV/ $c$ ) in the streamer chamber and  $\Delta p/p = 0.0005p$  for tracks also recon-

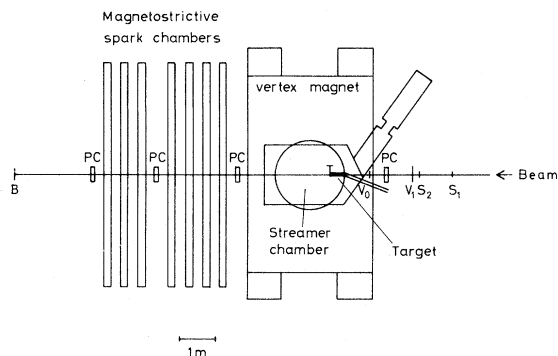


FIG. 1. Layout of the experiment.

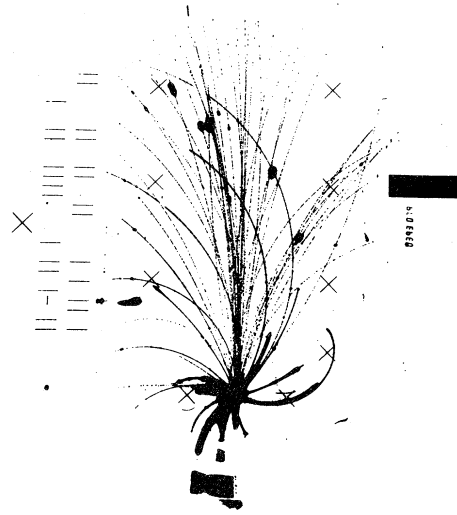


FIG. 2. Photograph of a  $pXe$  interaction at 200 GeV/ $c$  incident momentum.

structed in the spark chambers. About 10% of the charged tracks with momenta  $p > 30$  GeV/ $c$  had to be reconstructed from the streamer-chamber data alone.

The nuclear target consisted of a Mylar tube, 55 cm long, 3 cm in diameter, having a wall thickness of  $\sim 50$   $\mu$ m. It was filled with xenon or argon gas at 9 atm. Protons with momentum  $p$  less than 100 MeV/ $c$  or pions with  $p < 35$  MeV/ $c$  stop inside the target. The liquid hydrogen target was 36.5 cm long and 2 cm in diameter.

The incident beam was defined by a set of counters  $S_1, S_2$ . Upstream interactions were vetoed by counters  $V_0, V_1$  having a central hole. The beam was focused on a 2-cm-diameter scintillation counter  $B$ , positioned 10 m downstream of the target. The interaction trigger was a  $S_1 \cdot S_2 \cdot \bar{V}_0 \cdot \bar{V}_1 \cdot \bar{B}$  coincidence, which corresponded to four-momentum transfers  $|t| > 0.042$  (GeV/ $c$ )<sup>2</sup>. From a Monte Carlo calculation we estimate that this condition vetoed about 3% of inelastic events.

## III. DATA ANALYSIS

Table I shows for the different reactions the number of pictures analyzed and the resulting number of events within the fiducial volume. For  $pXe$  reactions 30% of the photographs had a good interaction in the target. The remaining pictures consisted of blank frames (1%), very faint images (2%), one-prong events or beam tracks (51%), events outside the fiducial volume (8%), multiple

TABLE I. The number of pictures analyzed and the resulting number of events within the fiducial region.

Reaction	Pictures	Events
$pp$	9400	3602
$pAr$	2000	383
$pXe$	4000	1194
$\bar{p}p$	5600	1856
$\bar{p}Ar$	3600	577
$\bar{p}Xe$	3500	905

interactions inside the target (6%), and failed geometry reconstruction (2%). The film was measured partly on image-plane digitizers, and partly on semiautomatic film-plane measuring machines (SWEEPNIK).

Careful checks were made for multiple interactions. All tracks apparently coming from a single vertex (the vertex itself is not visible) were measured and reconstructed. Any event which had one or more tracks coming from the target but not from the vertex was rejected from the sample.

Range, ionization, and decay signature were used to identify particles. From the ionization information of the streamer-chamber pions could be distinguished from protons in the momentum range  $150 < p < 600$  MeV/c and for dip angles less than 70 degrees. This information was used only for positive particles.

#### IV. EXPERIMENTAL RESULTS

In this section the experimental results on cross sections, multiplicities, rapidity distributions, and correlations will be presented for the reactions

- (1)  $p + p \rightarrow \text{anything}$ ,
- (2)  $\bar{p} + p \rightarrow \text{anything}$ ,
- (3)  $p + Ar \rightarrow \text{anything}$ ,
- (4)  $\bar{p} + Ar \rightarrow \text{anything}$ ,
- (5)  $p + Xe \rightarrow \text{anything}$ ,
- (6)  $\bar{p} + Xe \rightarrow \text{anything}$ .

##### A. Cross sections

The cross sections, uncorrected for trigger acceptance, are summarized in Table II. The measured  $pp$  cross section for charged multiplicity larger than two is  $28.1 \pm 0.5$  mb. The corresponding cross section obtained from bubble-chamber experiments

TABLE II. Cross sections uncorrected for trigger acceptance.

Reaction	Cross section (mb)
$pp$	$32.5 \pm 0.5$
$\bar{p}p$	$34.2 \pm 0.5$
$pAr$	$543 \pm 24$
$\bar{p}Ar$	$540 \pm 18$
$pXe$	$1212 \pm 35$
$\bar{p}Xe$	$1255 \pm 34$

is 29.2 mb.<sup>5</sup> This difference is in reasonable agreement with that expected from the trigger cutoff. The absorption cross sections of  $p$  and  $\bar{p}$  on argon and xenon are also slightly lower than measured elsewhere.<sup>6</sup>

##### B. Multiplicity distributions

In the following  $n_p$  is the number of identified protons. This number is not identical to the number of grey tracks  $n_g$  measured in emulsion experiments, however it characterizes the events in a similar way.<sup>2</sup> The particles below 600 MeV/c which are not identified as protons and all particles with momenta larger than 600 MeV/c are treated as  $\pi$  mesons and are referred to as "produced particles." The protons, which result from the deexcitation of the nucleus after the end of the interactions of the projectile, so-called evaporation particles, are mostly below 200 MeV/c (Ref. 7) and predominantly stop in the target.

In Figs. 3(a)–3(f) the multiplicity distributions are shown for all charged particles, excluding one-prong events, and in Figs. 3(g)–3(l) for negative particles only. All distributions are much broader than a Poisson distribution. The solid lines represent Koba-Nielsen-Olesen (KNO) distributions<sup>8</sup> for the observed average multiplicity  $\langle n \rangle$ . We used the parametrization obtained by a phenomenological fit to the multiplicity distributions of  $pp$  interactions at different energies<sup>9</sup>:

$$\psi(z) = \langle n \rangle \frac{\sigma_n}{\sigma_{\text{inel}}} = (3.79z + 33.7z^3 - 6.64z^5 + 0.332z^7)e^{-3.04z},$$

with  $z = n/\langle n \rangle$  and  $\sigma_n$  the topological cross section. In the case of the negative multiplicity distributions  $z$  is given by  $(2n_- + 2)/(2\langle n_- \rangle + 2)$  and by  $(2n_-)/(2\langle n_- \rangle)$  for  $p$  and  $\bar{p}$  reactions, respec-

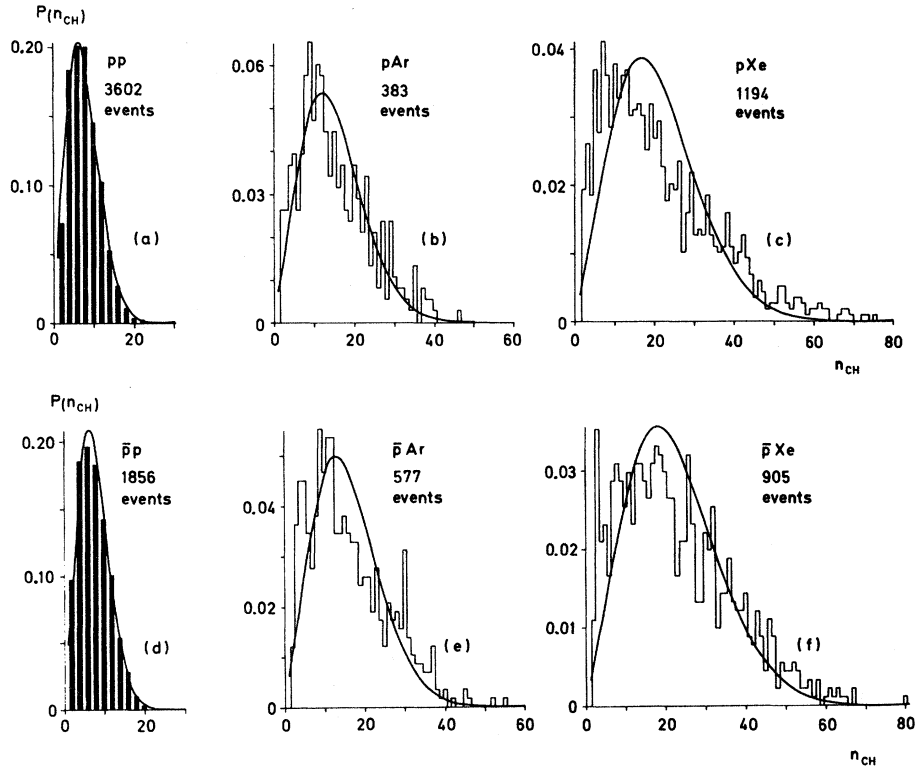


FIG. 3. Multiplicity distributions for (a)–(f) all charged particles ( $n_{CH}$ ) and (g)–(l) negative particles ( $n_-$ ), excluding one-prong events. The solid lines represent the KNO distribution obtained from a phenomenological fit to the multiplicity distributions in  $pp$  interactions (Ref. 9).

tively. From Figs. 3(g)–3(l) it is seen that this parametrization is consistent with the negative multiplicity distributions. On the other hand it does not describe the multiplicity distribution of all charged particles for the reactions on nuclear tar-

gets. The KNO-type behavior indicates correlations between the particles.

Table III summarizes the average multiplicities  $\langle n \rangle$ , dispersions  $D = [\langle (n - \langle n \rangle)^2 \rangle]^{1/2}$ , and skewness  $S = [\langle (n - \langle n \rangle)^3 \rangle]^{1/3}$  of the multiplicity dis-

TABLE III. Average multiplicity  $\langle n \rangle$ , dispersion  $D = [\langle (n - \langle n \rangle)^2 \rangle]^{1/2}$ , and skewness  $S = [\langle (n - \langle n \rangle)^3 \rangle]^{1/3}$  of the multiplicity distributions.

Target	Beam	All particles		Produced particles		Negative particles	
		$p$	$\bar{p}$	$p$	$\bar{p}$	$p$	$\bar{p}$
$p$	$\langle n \rangle$	$7.84 \pm 0.06$	$7.69 \pm 0.09$	$7.67 \pm 0.07$	$7.53 \pm 0.09$	$2.96 \pm 0.03$	$3.90 \pm 0.05$
	$D$	$3.84 \pm 0.05$	$3.89 \pm 0.06$	$3.93 \pm 0.05$	$3.98 \pm 0.06$	$1.92 \pm 0.03$	$1.95 \pm 0.03$
	$S$	$3.39 \pm 0.13$	$3.14 \pm 0.16$	$3.36 \pm 0.14$	$3.11 \pm 0.17$	$1.70 \pm 0.07$	$1.57 \pm 0.08$
Ar	$\langle n \rangle$	$14.98 \pm 0.45$	$16.01 \pm 0.40$	$13.31 \pm 0.38$	$14.23 \pm 0.35$	$5.39 \pm 0.17$	$6.80 \pm 0.16$
	$D$	$8.73 \pm 0.33$	$9.69 \pm 0.30$	$7.72 \pm 0.29$	$8.53 \pm 0.26$	$3.40 \pm 0.13$	$3.76 \pm 0.11$
	$S$	$8.08 \pm 0.74$	$8.96 \pm 0.74$	$7.44 \pm 0.72$	$8.05 \pm 0.69$	$3.16 \pm 0.31$	$3.28 \pm 0.32$
Xe	$\langle n \rangle$	$20.67 \pm 0.40$	$22.41 \pm 0.46$	$17.33 \pm 0.31$	$18.85 \pm 0.36$	$6.84 \pm 0.13$	$8.54 \pm 0.15$
	$D$	$13.87 \pm 0.33$	$13.82 \pm 0.34$	$10.96 \pm 0.25$	$11.08 \pm 0.26$	$4.41 \pm 0.11$	$4.58 \pm 0.11$
	$S$	$13.79 \pm 0.69$	$12.45 \pm 0.83$	$11.09 \pm 0.60$	$10.02 \pm 0.75$	$4.18 \pm 0.26$	$3.90 \pm 0.30$

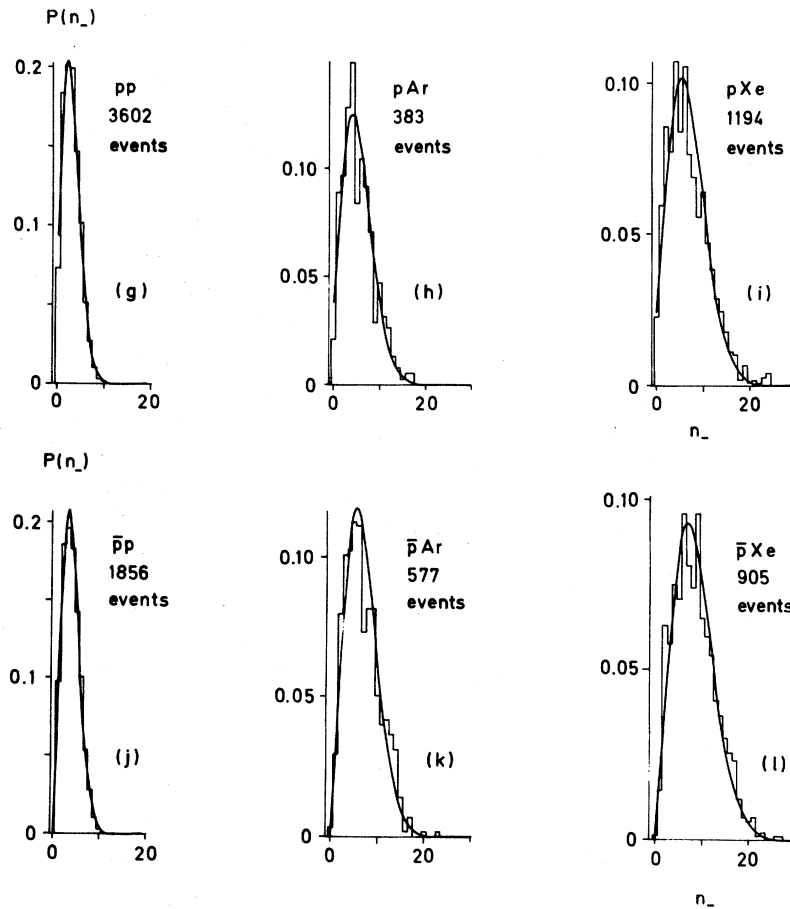


FIG. 3. (Continued.)

tributions for reactions (1)–(6). The average multiplicity is the same within errors for  $\bar{p}p$  and  $pp$  collisions at our energy but it is systematically higher for  $\bar{p}$ -nucleus collisions. This difference becomes larger with an increasing mass number of the nuclear target and indicates an increase of the probability of annihilation processes relative to

nonannihilation processes.<sup>10</sup>

Figure 4 shows the ratio  $R_A = \langle n \rangle_A / \langle n \rangle_p$  as a function of  $\bar{\nu}$ , where  $\langle n \rangle_A$  and  $\langle n \rangle_p$  are the average produced particle multiplicities on a nuclear and hydrogen target and where  $A$  is the mass number of the nucleus. The variable  $\bar{\nu}$  is defined as

$$\bar{\nu} = A\sigma_p / \sigma_A, \quad (7)$$

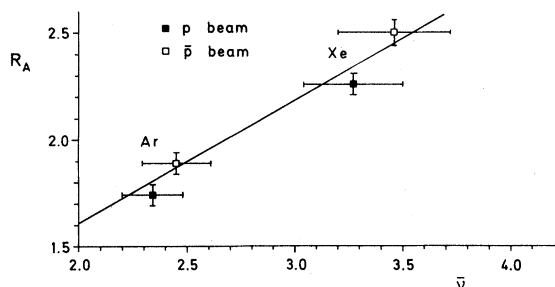


FIG. 4.  $R_A = \langle n \rangle_A / \langle n \rangle_p$  as a function of  $\bar{\nu}$  [see Eq. (7)]. The line shows the result of a fit (Ref. 11) to previous data on proton-nucleus collisions at 200 GeV/c.

with  $\sigma_p$  and  $\sigma_A$  the inelastic cross sections on protons and nuclei, respectively ( $\bar{\nu}_{Ar} = 2.3$ ,  $\bar{\nu}_{Xe} = 3.3$  for a proton beam from the cross sections of Ref. 6). The ratio  $R_A$  rises linearly with  $\bar{\nu}$  in agreement with previous experiments<sup>11</sup> represented by the solid line in Fig. 4.

The dispersion  $D_-$  as a function of the average multiplicity  $\langle n_- \rangle$  is shown in Fig. 5. It is interesting to note that the  $D_-$  and  $\langle n_- \rangle$  values for different nuclei at the same energy fall on the same straight line as first observed by Wroblewski<sup>12</sup> for  $pp$  reactions at different energies. Similar behavior is seen for  $\bar{p}$  beams and has been found previously

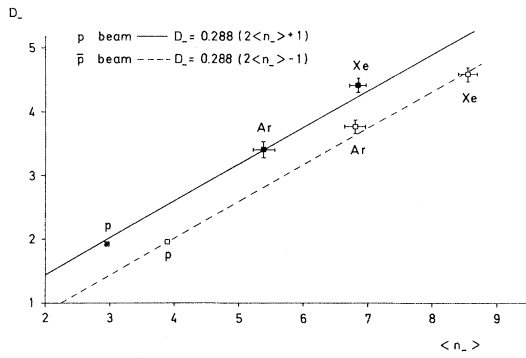


FIG. 5. Dispersion  $D_-$  for negative particles as a function of the average multiplicity  $\langle n_- \rangle$  for proton (full squares) and antiproton (open squares) interactions. The straight lines show the Wroblewski relation for  $pp$  interactions (Ref. 12)  $D = 2D_- = 0.576 (\langle n_{CH} \rangle - 1)$  where  $n_{CH} = 2n_- + 2$  was used for  $p$  and  $n_{CH} = 2n_-$  for  $\bar{p}$  reactions.

for  $\pi^-$  beams.<sup>11</sup>

The similarity of the  $D$  vs  $\langle n \rangle$  plots for nuclear and elementary targets was interpreted in Ref. 13 as a compensation of two effects:

- (i) The multiplicity distribution is broadened because it is a superposition of events with a different number of collisions  $\nu$ .
- (ii) For a fixed number of independent collisions  $\nu$  the ratio  $D/\langle n \rangle$  decreases as  $1/\sqrt{\nu}$ .

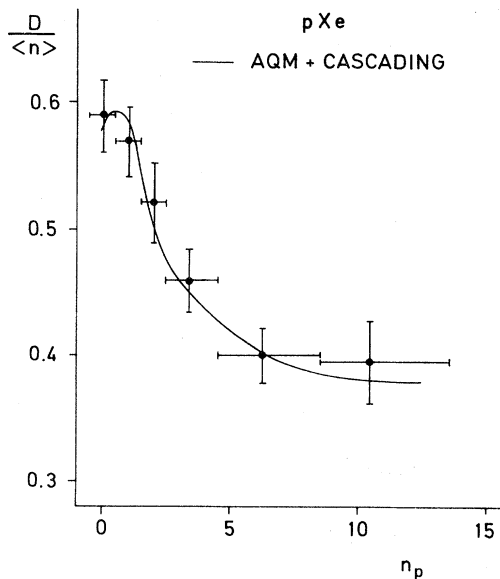


FIG. 6.  $D/\langle n \rangle$  as a function of the number of identified protons  $n_p$ . The solid line is the prediction of the AQM (Ref. 25).

This idea can be tested by studying  $D/\langle n \rangle$  as a function of  $\nu$ . Our attempt at such an analysis is shown in Fig. 6 where  $D/\langle n \rangle$  is plotted versus  $n_p$ , which can be considered as a measure of the number of collisions. For small  $n_p$  this ratio is close to the value for proton-proton reactions,<sup>14</sup> but it decreases with increasing  $n_p$  as expected.

Figures 7(a) and 7(b) show the average multiplicity of produced particles  $\langle n \rangle$  and negative particles  $\langle n_- \rangle$  in  $pXe$  and  $\bar{p}Xe$  events versus the number  $n_p$  of identified protons. At high values of  $n_p$  the average multiplicity has a value about three times that at  $n_p = 0$ , as naively expected in a model of three independently interacting quarks in the projectile. However, the saturation expected from such a model is not observed.

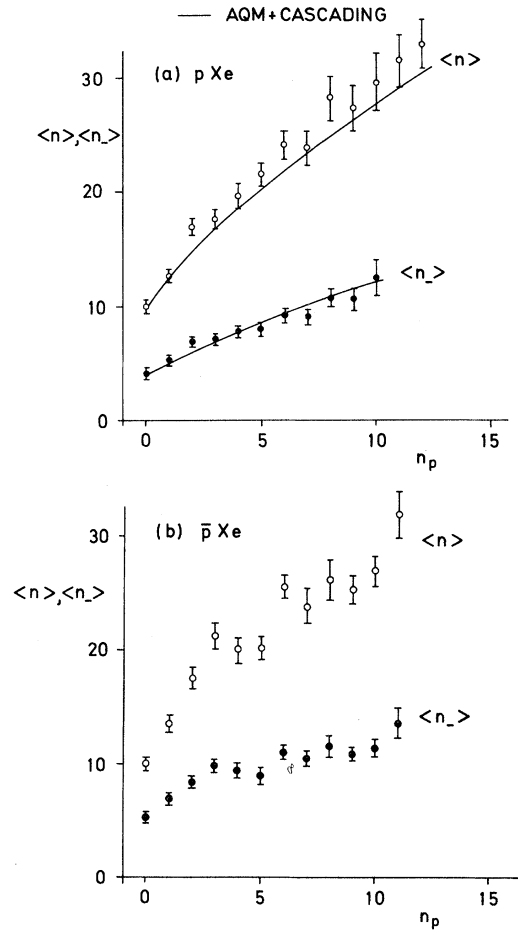


FIG. 7. Average multiplicity of produced particles  $\langle n \rangle$  (open circles) and negative particles  $\langle n_- \rangle$  (full circles) in (a)  $pXe$  and (b)  $\bar{p}Xe$  interactions as a function of the number of identified protons  $n_p$ . The solid lines are predictions of the AQM (Ref. 25).

TABLE IV. Normalized rapidity distribution  $(1/N_{ev})dN/dy$  of charged particles in the reactions  $pp, p\bar{p}, pAr, \bar{p}Ar, pXe, \bar{p}Xe \rightarrow X$  at 200 GeV/c.

$y$	All	Produced	Positive	Negative
		$pp \rightarrow X$		
-2.0	0.0±0.0	0.0±0.0	0.0±0.0	0.0±0.0
-1.5	0.001±0.001	0.001±0.001	0.001±0.001	0.0±0.0
-1.0	0.010±0.003	0.010±0.003	0.009±0.003	0.001±0.001
-0.5	0.069±0.007	0.069±0.007	0.054±0.006	0.015±0.003
0.0	0.641±0.019	0.290±0.013	0.545±0.017	0.095±0.008
0.5	0.684±0.019	0.682±0.019	0.447±0.016	0.237±0.011
1.0	1.200±0.026	1.200±0.026	0.786±0.021	0.415±0.015
1.5	1.568±0.029	1.568±0.029	0.941±0.023	0.626±0.019
2.0	1.656±0.030	1.656±0.030	0.960±0.023	0.696±0.020
2.5	1.776±0.031	1.776±0.031	0.981±0.023	0.795±0.021
3.0	1.771±0.031	1.771±0.031	0.956±0.023	0.816±0.021
3.5	1.659±0.030	1.659±0.030	0.915±0.023	0.744±0.020
4.0	1.468±0.029	1.468±0.029	0.832±0.021	0.636±0.019
4.5	1.112±0.025	1.112±0.025	0.693±0.020	0.419±0.015
5.0	0.819±0.021	0.819±0.021	0.555±0.017	0.264±0.012
5.5	0.538±0.017	0.538±0.017	0.429±0.015	0.109±0.008
6.0	0.422±0.015	0.422±0.015	0.389±0.014	0.033±0.004
6.5	0.205±0.010	0.205±0.010	0.193±0.010	0.012±0.003
7.0	0.081±0.006	0.081±0.006	0.078±0.006	0.003±0.001
7.5	0.023±0.003	0.023±0.003	0.022±0.003	0.001±0.001
8.0		$\bar{p}p \rightarrow X$		
-2.0	0.0±0.0	0.0±0.0	0.0±0.0	0.0±0.0
-1.5	0.0±0.0	0.0±0.0	0.0±0.0	0.0±0.0
-1.0	0.015±0.005	0.015±0.005	0.014±0.004	0.001±0.001
-0.5	0.064±0.009	0.064±0.009	0.042±0.007	0.022±0.006
0.0	0.693±0.027	0.346±0.020	0.586±0.025	0.107±0.011

TABLE IV. (Continued.)

$y$	All	Produced $\bar{p}p \rightarrow X$	Positive	Negative
0.5	$0.706 \pm 0.028$	$0.705 \pm 0.027$	$0.448 \pm 0.022$	$0.258 \pm 0.017$
1.0	$1.162 \pm 0.035$	$1.162 \pm 0.035$	$0.714 \pm 0.028$	$0.449 \pm 0.022$
1.5	$1.427 \pm 0.039$	$1.427 \pm 0.039$	$0.847 \pm 0.030$	$0.580 \pm 0.025$
2.0	$1.596 \pm 0.041$	$1.596 \pm 0.041$	$0.889 \pm 0.031$	$0.707 \pm 0.028$
2.5	$1.705 \pm 0.043$	$1.705 \pm 0.043$	$0.890 \pm 0.031$	$0.815 \pm 0.030$
3.0	$1.694 \pm 0.043$	$1.694 \pm 0.043$	$0.842 \pm 0.030$	$0.852 \pm 0.030$
3.5	$1.576 \pm 0.041$	$1.576 \pm 0.041$	$0.729 \pm 0.028$	$0.848 \pm 0.030$
4.0	$1.448 \pm 0.039$	$1.448 \pm 0.039$	$0.664 \pm 0.027$	$0.784 \pm 0.029$
4.5	$1.082 \pm 0.034$	$1.082 \pm 0.034$	$0.470 \pm 0.022$	$0.612 \pm 0.026$
5.0	$0.852 \pm 0.030$	$0.852 \pm 0.030$	$0.276 \pm 0.017$	$0.575 \pm 0.025$
5.5	$0.572 \pm 0.025$	$0.572 \pm 0.025$	$0.138 \pm 0.012$	$0.434 \pm 0.021$
6.0	$0.412 \pm 0.021$	$0.412 \pm 0.021$	$0.053 \pm 0.008$	$0.358 \pm 0.019$
6.5	$0.261 \pm 0.016$	$0.261 \pm 0.016$	$0.011 \pm 0.003$	$0.251 \pm 0.015$
7.0	$0.105 \pm 0.010$	$0.105 \pm 0.010$	$0.004 \pm 0.002$	$0.101 \pm 0.010$
7.5	$0.030 \pm 0.005$	$0.030 \pm 0.005$	$0.0 \pm 0.0$	$0.030 \pm 0.005$
8.0				
		$p \text{ Ar} \rightarrow X$		
-2.0	$0.0 \pm 0.0$	$0.0 \pm 0.0$	$0.0 \pm 0.0$	$0.0 \pm 0.0$
-1.5	$0.042 \pm 0.015$	$0.037 \pm 0.014$	$0.031 \pm 0.013$	$0.010 \pm 0.007$
-1.0	$0.183 \pm 0.031$	$0.172 \pm 0.030$	$0.151 \pm 0.028$	$0.031 \pm 0.013$
-0.5	$1.689 \pm 0.094$	$0.812 \pm 0.065$	$1.381 \pm 0.085$	$0.308 \pm 0.040$
0.0	$3.346 \pm 0.132$	$1.573 \pm 0.091$	$2.889 \pm 0.123$	$0.457 \pm 0.049$
0.5	$2.068 \pm 0.104$	$2.047 \pm 0.103$	$1.342 \pm 0.084$	$0.726 \pm 0.062$
1.0	$2.527 \pm 0.115$	$2.527 \pm 0.115$	$1.556 \pm 0.090$	$0.971 \pm 0.071$
1.5	$2.924 \pm 0.124$	$2.924 \pm 0.124$	$1.692 \pm 0.094$	$1.232 \pm 0.080$
2.0	$2.935 \pm 0.124$	$2.935 \pm 0.124$	$1.681 \pm 0.094$	$1.253 \pm 0.081$
2.5	$3.217 \pm 0.130$	$3.217 \pm 0.130$	$1.671 \pm 0.093$	$1.546 \pm 0.090$
3.0	$3.039 \pm 0.126$	$3.039 \pm 0.126$	$1.713 \pm 0.095$	$1.326 \pm 0.083$
3.5	$2.282 \pm 0.109$	$2.282 \pm 0.109$	$1.352 \pm 0.084$	$0.930 \pm 0.070$
4.0				

TABLE IV. (Continued.)

$y$	All	Produced $p\text{Ar} \rightarrow X$	Positive	Negative
4.5	$2.120 \pm 0.105$	$2.120 \pm 0.105$	$1.154 \pm 0.078$	$0.966 \pm 0.071$
5.0	$1.467 \pm 0.088$	$1.467 \pm 0.088$	$0.924 \pm 0.069$	$0.543 \pm 0.053$
5.5	$0.914 \pm 0.069$	$0.914 \pm 0.069$	$0.601 \pm 0.056$	$0.313 \pm 0.040$
6.0	$0.491 \pm 0.051$	$0.491 \pm 0.051$	$0.381 \pm 0.045$	$0.110 \pm 0.024$
6.5	$0.292 \pm 0.039$	$0.292 \pm 0.039$	$0.235 \pm 0.035$	$0.057 \pm 0.017$
7.0	$0.141 \pm 0.027$	$0.141 \pm 0.027$	$0.141 \pm 0.027$	$0.0 \pm 0.0$
7.5	$0.073 \pm 0.020$	$0.073 \pm 0.020$	$0.073 \pm 0.020$	$0.0 \pm 0.0$
8.0	$0.026 \pm 0.012$	$0.026 \pm 0.012$	$0.026 \pm 0.012$	$0.0 \pm 0.0$
		$\bar{p}\text{Ar} \rightarrow X$		
-2.0	$0.007 \pm 0.005$	$0.007 \pm 0.005$	$0.007 \pm 0.005$	$0.0 \pm 0.0$
-1.5	$0.031 \pm 0.010$	$0.031 \pm 0.010$	$0.031 \pm 0.010$	$0.0 \pm 0.0$
-1.0	$0.226 \pm 0.028$	$0.219 \pm 0.028$	$0.156 \pm 0.023$	$0.069 \pm 0.016$
-0.5	$1.738 \pm 0.078$	$0.846 \pm 0.054$	$1.462 \pm 0.071$	$0.276 \pm 0.031$
0.0	$3.606 \pm 0.112$	$1.674 \pm 0.076$	$3.027 \pm 0.103$	$0.578 \pm 0.045$
0.5	$2.444 \pm 0.092$	$2.420 \pm 0.092$	$1.552 \pm 0.073$	$0.892 \pm 0.056$
1.0	$3.153 \pm 0.105$	$3.149 \pm 0.105$	$1.924 \pm 0.082$	$1.229 \pm 0.065$
1.5	$3.222 \pm 0.106$	$3.222 \pm 0.106$	$1.882 \pm 0.081$	$1.340 \pm 0.068$
2.0	$3.188 \pm 0.105$	$3.188 \pm 0.105$	$1.726 \pm 0.077$	$1.462 \pm 0.071$
2.5	$3.122 \pm 0.104$	$3.122 \pm 0.104$	$1.656 \pm 0.076$	$1.465 \pm 0.071$
3.0	$2.878 \pm 0.100$	$2.878 \pm 0.100$	$1.382 \pm 0.069$	$1.497 \pm 0.072$
3.5	$2.476 \pm 0.093$	$2.476 \pm 0.093$	$1.201 \pm 0.065$	$1.274 \pm 0.067$
4.0	$1.986 \pm 0.083$	$1.986 \pm 0.083$	$0.910 \pm 0.056$	$1.076 \pm 0.061$
4.5	$1.608 \pm 0.075$	$1.608 \pm 0.075$	$0.653 \pm 0.048$	$0.955 \pm 0.058$
5.0	$0.997 \pm 0.059$	$0.997 \pm 0.059$	$0.382 \pm 0.036$	$0.615 \pm 0.046$
5.5	$0.569 \pm 0.044$	$0.569 \pm 0.044$	$0.149 \pm 0.023$	$0.420 \pm 0.038$
6.0	$0.281 \pm 0.031$	$0.281 \pm 0.031$	$0.038 \pm 0.012$	$0.243 \pm 0.029$
6.5	$0.153 \pm 0.023$	$0.153 \pm 0.023$	$0.003 \pm 0.003$	$0.149 \pm 0.023$
7.0	$0.087 \pm 0.017$	$0.087 \pm 0.017$	$0.0 \pm 0.0$	$0.087 \pm 0.017$
7.5				

TABLE IV. (Continued.)

$y$	All	Produced $\bar{p}\text{Ar}\rightarrow X$	Positive	Negative
8.0	0.014±0.007	0.014±0.007	0.0±0.0	0.014±0.007
		$p\text{Xe}\rightarrow X$		
-2.0	0.015±0.005	0.015±0.005	0.013±0.005	0.002±0.002
-1.5	0.075±0.011	0.075±0.011	0.065±0.010	0.010±0.004
-1.0	0.392±0.026	0.381±0.025	0.312±0.023	0.080±0.012
-0.5	3.347±0.075	1.283±0.046	2.963±0.070	0.384±0.025
0.0	6.489±0.104	2.574±0.066	5.694±0.098	0.795±0.037
0.5	3.418±0.076	3.365±0.075	2.273±0.062	1.145±0.044
1.0	3.961±0.081	3.961±0.081	2.486±0.065	1.475±0.050
1.5	4.151±0.083	4.151±0.083	2.540±0.065	1.611±0.052
2.0	3.896±0.081	3.896±0.081	2.215±0.061	1.681±0.053
2.5	3.738±0.079	3.738±0.079	2.097±0.059	1.641±0.052
3.0	3.346±0.075	3.346±0.075	1.790±0.055	1.556±0.051
3.5	2.917±0.070	2.917±0.070	1.613±0.052	1.304±0.047
4.0	2.173±0.060	2.173±0.060	1.224±0.045	0.949±0.040
4.5	1.420±0.049	1.420±0.049	0.857±0.038	0.563±0.031
5.0	0.924±0.039	0.924±0.039	0.634±0.033	0.290±0.022
5.5	0.518±0.029	0.518±0.029	0.391±0.026	0.127±0.015
6.0	0.255±0.021	0.255±0.021	0.226±0.019	0.028±0.007
6.5	0.109±0.014	0.109±0.014	0.104±0.013	0.005±0.003
7.0	0.030±0.007	0.030±0.007	0.030±0.007	0.0±0.0
7.5	0.003±0.002	0.003±0.002	0.003±0.002	0.0±0.0
8.0		$\bar{p}\text{Xe}\rightarrow X$		
-2.0	0.013±0.005	0.013±0.005	0.013±0.005	0.0 ±0.0
-1.5	0.086±0.014	0.086±0.014	0.077±0.013	0.009±0.004
-1.0	0.469±0.032	0.458±0.032	0.376±0.029	0.093±0.014
-0.5	3.628±0.090	1.275±0.053	3.266±0.085	0.361±0.028
0.0	6.993±0.124	2.720±0.078	6.078±0.116	0.915±0.045

TABLE IV. (Continued.)

$y$	All	Produced	Positive	Negative
		$\bar{p} \text{Xe} \rightarrow X$		
0.5	3.905±0.093	3.863±0.092	2.502±0.074	1.403±0.056
1.0	4.336±0.098	4.336±0.098	2.695±0.077	1.642±0.060
1.5	4.383±0.098	4.383±0.098	2.617±0.076	1.765±0.062
2.0	4.389±0.099	4.389±0.099	2.460±0.074	1.929±0.065
2.5	3.885±0.093	3.885±0.093	2.075±0.068	1.810±0.063
3.0	3.423±0.087	3.423±0.087	1.664±0.061	1.759±0.062
3.5	3.062±0.082	3.062±0.082	1.555±0.059	1.507±0.058
4.0	2.372±0.072	2.372±0.072	1.086±0.049	1.285±0.053
4.5	1.577±0.059	1.577±0.059	0.657±0.038	0.920±0.045
5.0	1.066±0.049	1.066±0.049	0.336±0.027	0.730±0.040
5.5	0.564±0.035	0.564±0.035	0.137±0.017	0.427±0.031
6.0	0.296±0.026	0.296±0.026	0.031±0.008	0.265±0.024
6.5	0.170±0.019	0.170±0.019	0.011±0.005	0.159±0.019
7.0	0.066±0.012	0.066±0.012	0.0±0.0	0.066±0.012
7.5	0.022±0.007	0.022±0.007	0.0±0.0	0.022±0.007
8.0				

### C. Rapidity distributions

Throughout this paper the rapidity

$$y = \frac{1}{2} \ln[(E + p_{||})/(E - p_{||})]$$

in the laboratory system is used. The center-of-mass-system (c.m.s.) rapidity is shifted by 3 units, assuming collisions on a free proton. The rapidity distributions were measured in the full rapidity range from  $-2.0$  to  $8.0$ . In Table IV the normalized rapidity distributions

$$\rho(y) = \frac{1}{N_{ev}} \frac{dN}{dy}$$

for all particles, for all produced particles, for positive and negative particles in the reactions (1)–(6) are given. Here  $N_{ev}$  is the number of events and  $N$  the number of particles in these events. The limited identification of protons leads to a distortion of the rapidity distribution. We investigated this bias for rapidity  $y > 4$ . For this purpose the rapidity

distribution was also calculated when assigning to the fastest particle with the charge of the beam a nucleon mass, if it had  $x_F$  ( $x_F = p_{||}/p_{inc}$ ) larger than the maximal  $x_F$  observed for the opposite sign particles (i.e., Feynman  $x_F > 0.44$  for  $pp$  and  $x_F > 0.31$  for  $pXe$  reactions). The comparison of the rapidity distributions is shown in Fig. 8 for the case of  $pp$  and  $pXe$  scattering as an example. The effect of particle misidentification is approximately the same in  $pp$  as in  $pXe$  reactions and thus practically cancels in the ratio  $R(y)$  of the rapidity distributions where

$$R(y) = \rho_A(y) / \rho_p(y)$$

(the subscript of  $\rho$  indicates the type of target).

Figure 9 shows for protons and antiprotons incident on argon and xenon targets the ratio  $R(y)$  versus laboratory rapidity. The common characteristics of the presented ratios  $R(y)$  are as follows.

(i) Very large values in the target fragmentation region ( $y < 1$ ). As seen from Figs. 9(a)–9(d) these

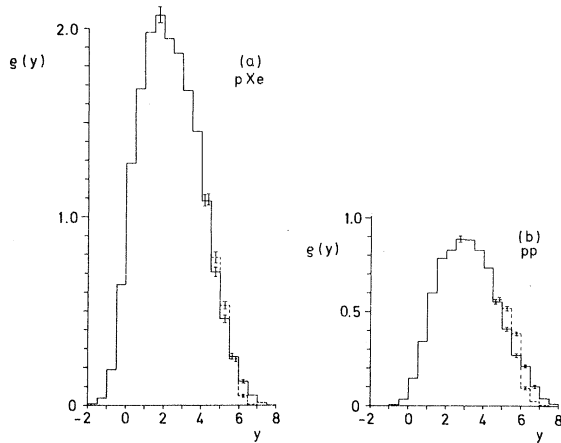


FIG. 8. Rapidity distributions for (a)  $pXe$  and (b)  $pp$  scattering assuming that all particles in the projectile fragmentation region are pions (solid line histograms), and assuming that the fastest particle with  $x_F \gtrsim 0.4$  is a proton (dashed histograms).

values exceed significantly the average number of collisions  $\bar{\nu}$ . This is evidence for intranuclear cascading.

(ii) In the rapidity region  $1 < y < 5$ ,  $R(y)$  shows a slow decrease with increasing  $y$ . The  $A$  dependence

of  $R(y)$  in the central region ( $2 < y < 4$ ) is slower than that of  $\bar{\nu}$ . The measured ratios are  $R_{Xe}(y)/R_{Ar}(y) = 1.21 \pm 0.03$  for produced particles and  $1.22 \pm 0.04$  for negative particles whereas  $\bar{\nu}_{Xe}/\bar{\nu}_{Ar} = 1.40 \pm 0.02$ .<sup>6</sup>

(iii) In the projectile fragmentation region ( $y > 5$ ) the ratio  $R(y)$  falls below one, in agreement with earlier measurements.<sup>15</sup>

Figure 10 shows the ratio  $R_-(y)$  for negative particles produced in  $pXe$  and  $pp$  interactions versus rapidity. The features are similar to those observed for all produced particles. Using  $R_-(y)$  to investigate nuclear effects may be misleading, since the nucleus consists of protons and neutrons and the  $\pi^-$  spectra from neutron and proton fragmentation are different. Thus the  $\rho_p^-(y)$  in the denominator of  $R_-(y)$  would better be replaced by  $[\rho_p^-(y) + \rho_n^-(y)]/2$  for  $y < 3$ . Since we did not measure  $pn$  or  $pd$  interactions we used

$$[\rho_p^-(y) + \rho_p^+(y)]/2 = \rho_p(y)/2$$

instead. The crosses in Fig. 10 show the resulting  $\bar{R}_-(y)$ . It is now seen that this  $\bar{R}_-(y)$  shows a more pronounced plateau. Moreover cascading seems to be important only for values of  $y < 1.5$ .

Figure 11 shows  $R(y)$  for different values of  $n_p$  for  $pXe$  interactions. The large value in the target fragmentation region comes mainly from events

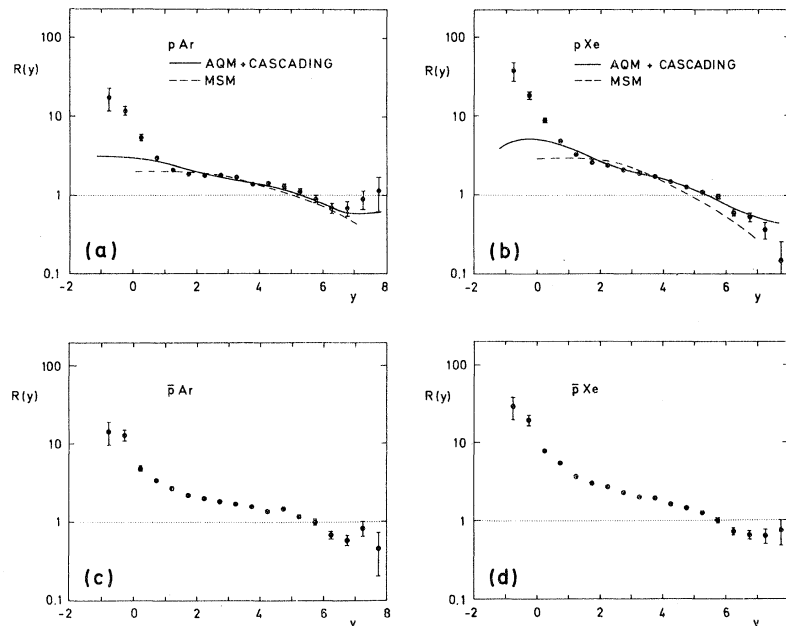


FIG. 9. The ratio  $R(y) = \rho_A(y)/\rho_p(y)$  for produced particles in (a)  $pAr$ , (b)  $pXe$ , (c)  $\bar{p}Ar$ , and (d)  $\bar{p}Xe$  reactions as a function of the rapidity  $y$ . The solid lines are the predictions of the AQM (Ref. 25), and the dashed lines those of the MSM (Ref. 20).

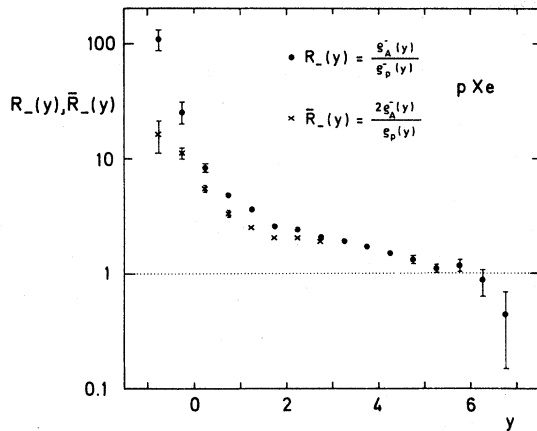


FIG. 10. The ratio  $R_-(y) = \rho_{\bar{X}e}(y) / \rho_p^-(y)$  for negative particles in  $pXe$  reactions as a function of the rapidity  $y$  (circles). Also shown (crosses) is  $R_-(y)$  with  $\rho_p^-$  symmetrized for  $y < 3$ , i.e.,  $[\rho_p^-(y) + \rho_p^+(y)]/2 = \rho_p(y)/2$  instead of  $\rho_p^-(y)$ .

with large values of  $n_p$ . This is further evidence for the importance of intranuclear cascading. For small  $n_p$  the values of  $R(y)$  approach one as would be expected for a reaction on a single nucleon. Similar behavior is observed for the other reactions of this experiment, i.e.,  $pAr$ ,  $\bar{p}Ar$ , and  $\bar{p}Xe$  collisions.

In Fig. 12 we show the ratio of  $R(y)$  for  $p$  and  $\bar{p}$  induced reactions on xenon. The ratio is about 0.9 and reflects the fact that the multiplicity is lower in  $p$  than in  $\bar{p}$  interactions with nuclei.

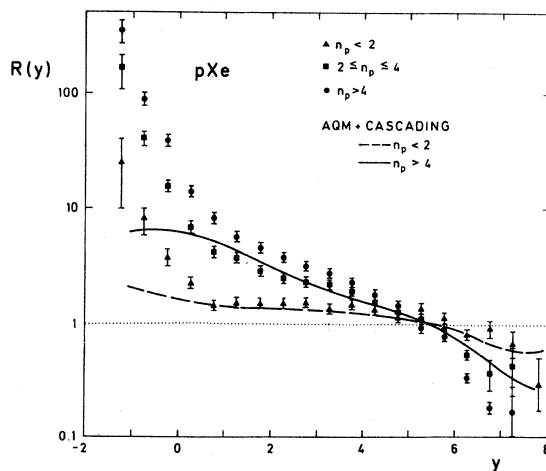


FIG. 11. The ratio  $R(y) = \rho_{Xe}(y) / \rho_p(y)$  for different numbers of identified protons  $n_p$  in  $pXe$  interactions.

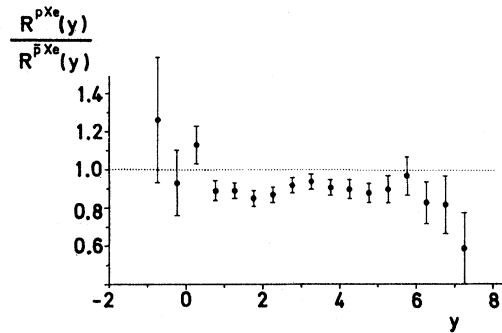


FIG. 12. The ratio of  $R(y)$  in  $pXe$  to that in  $\bar{p}Xe$  reactions, i.e.,  $(\rho_{pXe}/\rho_{pp}) / (\rho_{\bar{p}Xe}/\rho_{pp})$  as a function of rapidity  $y$ .

#### D. Correlations

As mentioned above, the KNO-type multiplicity distribution indicates correlations between particles. Figure 13 shows for  $pXe$  reactions the inclusive two-particle correlation function:

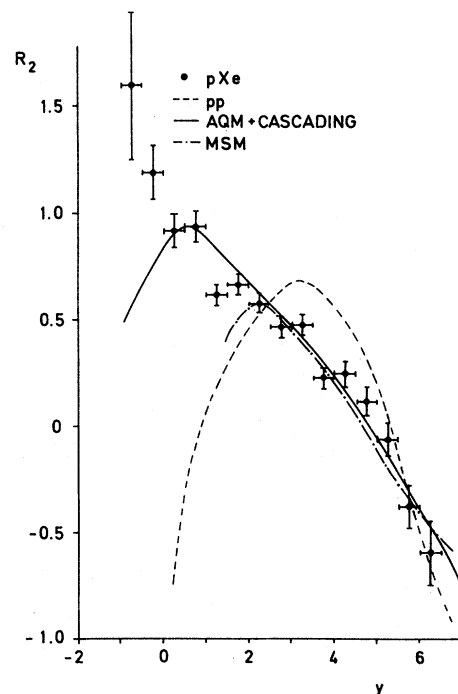


FIG. 13. The two-particle correlation function  $R_2(y_1, y_2) = \rho(y_1, y_2) / \rho(y_1)\rho(y_2) - 1$  for  $y = y_1 = y_2$  versus rapidity  $y$ . The data points show the results for  $pXe$  interactions and the dashed line represents the data for  $pp$  interactions from this experiment. The solid curve shows the prediction of the AQM (Ref. 25) and the dashed-dotted curve that of the MSM (Ref. 20).

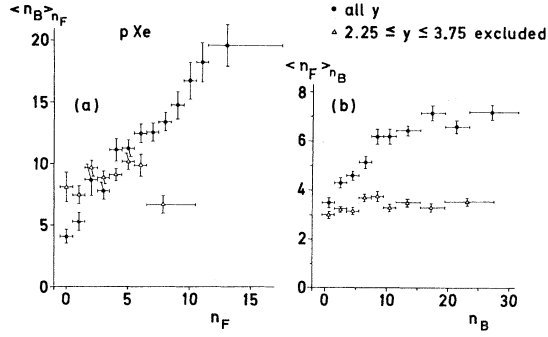


FIG. 14. (a) The average multiplicity  $\langle n_B \rangle$  in the backward hemisphere versus the multiplicity  $n_F$  in the forward hemisphere and (b)  $\langle n_F \rangle$  versus  $n_B$  for  $pXe$  reactions. The results without rapidity cut are shown by the circles and with exclusion of the central rapidity region  $2.25 \leq y \leq 3.75$  by the triangles.

$$R_2(y_1, y_2) = \frac{\rho(y_1, y_2)}{\rho(y_1)\rho(y_2)} - 1$$

at  $y_1 = y_2 = y$ , where

$$\rho_2(y_1, y_2) = \frac{1}{N_{ev}} \frac{d^2 N}{dy_1 dy_2}.$$

For comparison the dashed curve shows  $R_2$  for  $pp$  reactions. The prominent feature of the  $pXe$  data is a positive correlation for  $y < 1$ . This effect is a further indication of intranuclear cascading. In the central region,  $R_2$  is lower for the xenon than for the proton target. This is consistent with the assumption that particles produced in hadron nucleus collisions result from approximately independent multiple interactions.

Long-range correlations can be studied by investigating the correlations between the number  $n_B$  of particles in the backward c.m.s. hemisphere and the number of particles  $n_F$  in the forward c.m.s. hemisphere.<sup>16</sup> From Fig. 14, which shows  $\langle n_B \rangle$

versus  $n_F$  and  $\langle n_F \rangle$  versus  $n_B$  (circles) for  $pXe$  reactions, a strong correlation is seen. To minimize the effects of short-range correlations the results are also shown (triangles) after the elimination of particles in the central rapidity region  $2.25 < y < 3.75$ . With this cut the correlation almost disappears. This result indicates the presence of strong short-range correlations in the central region and only very weak long-range correlations between the two fragmentation regions defined as above. A similar behavior is seen in the  $pp$  data of this and previous experiments.<sup>16</sup> In Table V we present the slopes  $b$  obtained from fits of the expression

$$\langle n_B \rangle_{n_F} = \langle n_B \rangle + b(n_F - \langle n_F \rangle)$$

to the data of all six reactions. Also the average forward and backward multiplicities  $\langle n_F \rangle$  and  $\langle n_B \rangle$  are listed. The results are given with and without rapidity cut.

### E. Net charge distribution

The distributions of the average net charge

$$dQ/dy = \rho^+(y) - \rho^-(y)$$

as a function of rapidity are shown in Fig. 15 for  $\bar{p}p$  and  $\bar{p}Xe$  reactions. The following observations can be made.

(i) The average net charge is negative in the forward and positive in the backward direction, changing sign at a rapidity value close to  $y=3$  (corresponding to c.m.s. rapidity zero).

(ii) In the forward hemisphere, the distributions coincide, within errors, for  $\bar{p}p$  and  $\bar{p}Xe$  collisions, but they differ dramatically in the backward hemisphere.

TABLE V. Average multiplicity in the forward hemisphere  $\langle n_F \rangle$  and in the backward hemisphere  $\langle n_B \rangle$  and the parameter  $b$  obtained from a fit of the expression  $\langle n_B \rangle_{n_F} = \langle n_B \rangle + b(n_F - \langle n_F \rangle)$ .

Reaction	No rapidity cut			2.25 < y < 3.75 excluded		
	$\langle n_F \rangle$	$\langle n_B \rangle$	$b$	$\langle n_F \rangle$	$\langle n_B \rangle$	$b$
$pp$	4.00±0.04	3.68±0.04	0.215±0.023	2.71±0.03	2.36±0.03	0.054±0.024
$\bar{p}p$	3.97±0.06	3.56±0.06	0.267±0.034	2.72±0.04	2.30±0.04	0.017±0.035
$pAr$	5.37±0.15	8.16±0.33	0.73±0.08	3.25±0.09	5.81±0.25	0.15±0.13
$\bar{p}Ar$	5.45±0.12	8.97±0.29	1.11±0.07	3.40±0.08	6.63±0.23	0.50±0.10
$pXe$	5.75±0.09	11.75±0.28	1.23±0.07	3.35±0.05	8.96±0.23	-0.06±0.11
$\bar{p}Xe$	6.19±0.10	12.75±0.33	0.98±0.09	3.68±0.06	9.77±0.27	0.18±0.13

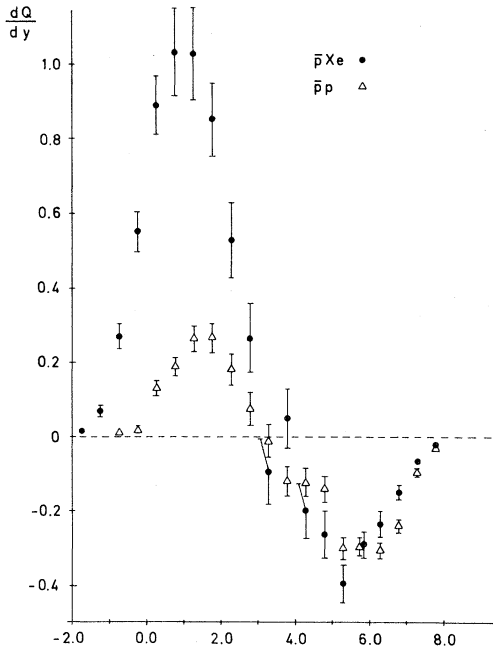


FIG. 15. The average net charge  $dQ/dy = \rho_+(y) - \rho_-(y)$  versus rapidity  $y$  for  $\bar{p}$ Xe (circles) and  $\bar{p}$ p (triangles) interactions.

The same features are also present in  $\bar{p}$ Ar data, as can be seen from Table VI, where the integrated average net charges are shown for each hemisphere for the  $\bar{p}$ p,  $\bar{p}$ Ar, and  $\bar{p}$ Xe data.

The observed smallness of the deviation of the forward integrated average net charge from  $-1$  indicates a good separation of the beam and target fragmentation at our energy.<sup>17</sup> The large positive net charge in the backward hemisphere for the Ar and Xe targets is a clear indication of the interactions of secondaries inside the nucleus. Indeed, in the absence of such interactions, one expects the integrated average net charge to be given by the average number of struck protons ( $=\bar{\nu}_A Z/A$ ). As seen from Table VI the measured values exceed this expectation by a large amount.

## V. COMPARISON WITH MODELS

We now compare the experimental results with predictions of two types of model formulated in the framework of the parton picture.

(i) Multiple-scattering models<sup>18–21</sup> (MSM's) where particle production is mainly determined by the average number of collisions  $\bar{\nu}$  as defined in expression (7).

(ii) Additive quark models<sup>22–25</sup> (AQM's), where particle production is determined by the number of interacting quarks in the projectile.

Both types of models use the relativistic multiple-scattering theory of Glauber and Gribov<sup>26</sup> in order to calculate the probability of obtaining a certain number of interactions of a nucleon inside the nucleus. For comparison with our data we have chosen a specific model of each type, where predictions, although incomplete, are available in the literature.

The MSM chosen is that of Refs. 19 and 20. It is based on the two-chain dual parton model of hadron-hadron interactions. Each colliding nucleon splits through gluon exchange into colored systems: a quark, a diquark, and sea quarks, which can have any number of interactions with the nucleus. Each colored system fragments by gluon exchange according to a universal fragmentation function. The dashed lines in Fig. 9(a) and 9(b) are predictions of the MSM. The central region is fairly well described, whereas in the projectile fragmentation region the predicted values are systematically too low, especially for xenon. The large discrepancy in the target fragmentation region occurs probably because cascading effects are neglected in the model. The predictions for the correlation  $R_2$  (dashed-dotted line in Fig. 13) agree well for  $y > 2$ .

In the AQM of Ref. 25, which we chose for comparison with our data, the proton is considered as usual to consist of three dressed quarks which independently interact in the sense of the additive

TABLE VI. The integrated average net charge  $Q$  in the forward and backward hemispheres for  $\bar{p}$ p,  $\bar{p}$ Ar, and  $\bar{p}$ Xe reactions. The mean number of struck protons in the nucleus  $\bar{\nu}_{A/Z}$  is shown for comparison.

Reaction	$\bar{\nu}_A Z/A$	Integrated average net charge $Q$		
		Produced particles	All particles	Forward
$\bar{p}$ p	1.0	$0.57 \pm 0.04$	$0.75 \pm 0.04$	$-0.83 \pm 0.04$
$\bar{p}$ Ar	$1.10 \pm 0.06$	$1.63 \pm 0.12$	$3.06 \pm 0.14$	$-0.81 \pm 0.10$
$\bar{p}$ Xe	$1.42 \pm 0.11$	$2.78 \pm 0.11$	$6.12 \pm 0.13$	$-0.83 \pm 0.08$

quark model. The probability for one, two, or three quarks interacting is calculated by using the Glauber-Gribov theory with the additional assumption that the quark-nucleon cross section is about 10 mb. Each quark-nucleon interaction is assumed to be independent and to be given by a phenomenological description of  $pp$  interactions. In addition to the primary interaction, cascading of slow particles is introduced using the concept of "formation length."<sup>27</sup> For a particle with momentum  $p$ , the formation length is assumed to be  $L_f = p/m_0^2$ , where  $m_0^2$  is a free parameter chosen<sup>25</sup> to have the value of  $0.65 \text{ GeV}^2$ . A produced particle is allowed to interact in the nucleus if its path length is larger than its formation length  $L_f$ . The solid lines in Figs. 6, 7, 9, 11, and 13 are predictions of the model. The model describes the data quite well for  $y > 0$ . Using simplified kinematics, the model cannot describe the data for  $y < 0$ . Furthermore, the behavior of  $R(y)$  for  $n_p > 4$ , shown in Fig. 11, is not satisfactorily described.

The weak  $A$  dependence of  $R(y)$  measured in the central region (see Sec. IV C) is characterized by the ratio

$$R_{Xe}(y)/R_{Ar}(y) = 1.21 \pm 0.03 .$$

This ratio is practically the same for all charged particles and for negative particles, and it can be determined with good accuracy. It is thus a good testing point for models. The naive expectation of the multiple-collision picture is

$$R_{Xe}(y)/R_{Ar}(y) = \bar{\nu}_{Xe}/\bar{\nu}_{Ar} = 1.40 \pm 0.02 ,$$

which is reduced to 1.3 by energy attenuation.<sup>18</sup> In the MSM (Ref. 20) the prediction is 1.3. In the AQM (Ref. 23) this ratio should be given by  $\bar{W}_{Xe}/\bar{W}_{Ar}$ , where  $\bar{W}_A$  is the average number of interacting quarks. The predicted value for  $R_{Xe}(y)/R_{Ar}(y)$  is 1.2. The data favor the AQM.

## VI. SUMMARY AND CONCLUSION

In this paper we presented data on 200-GeV/c  $pAr$ ,  $pXe$ ,  $\bar{p}Ar$ , and  $\bar{p}Xe$  reactions obtained with a streamer-chamber vertex spectrometer. The streamer chamber enabled us to measure for the first time charged-particle momenta over the whole solid angle and to identify slow protons. Multipli-

city distributions, the full inclusive rapidity spectra, and correlations of produced particles have been presented and compared to  $pp$  and  $\bar{p}p$  data from the same experiment. The dependence of these quantities on the number of identified slow protons  $n_p$ , assumed to be a measure of the number of interactions in the nucleus, was investigated.

The main results of this experiment are the following.

(a) No significant differences between  $p$  and  $\bar{p}$  interactions with nuclei are observed, except for the average multiplicity which is slightly larger for  $\bar{p}$  reactions.

(b) The multiplicity distributions of negative hadrons are all consistent with Slattery's parametrization of the KNO distribution of  $pp$  scattering. Correspondingly the values of  $D_-$  versus  $\langle n_- \rangle$  for the various reactions are consistent with the same straight line which was first observed by Wroblewski for  $pp$  scattering at different energies. On the other hand the multiplicity distributions of all charged particles on the nuclear targets are not well described by the  $pp$  KNO curve.

(c) The ratio  $D/\langle n \rangle$  for produced particles falls with increasing  $n_p$ . This may indicate that the multiplicity distribution on nuclei is a convolution of distributions from several independent particle-production processes as suggested by MSM and AQM models.

(d) From the analysis of the rapidity distributions it follows that in hadron-nucleus interactions cascading of slow secondaries is clearly present leading to a large number of particles in the target fragmentation region.

(e) The  $A$  dependence of  $R(y)$  in the central region is weaker than that of  $\bar{\nu}$ , in agreement with the AQM prediction.

(f) In the projectile fragmentation region there is a depletion of particles in interactions on nuclei compared to interactions on protons.

(g) From the forward and backward multiplicities it can be concluded that there are strong short-range correlations in the central region, whereas long-range correlations between the two fragmentation regions are very weak.

(h) The distribution of the average net charge in rapidity shows a rather good separation of the projectile and the target fragmentation regions.

Discrepancies emerge when comparing the detailed data of this experiment with the predictions of current models. In particular it appears from the data that cascading is an important effect which none of the models in their present form is able to describe satisfactorily.

## ACKNOWLEDGMENTS

It is a pleasure to acknowledge the excellent work of the engineers, the technicians, and the programming and measuring teams at the collaborating institutions. We wish to thank the staff at CERN for the operation of the SPS accelerator and the H2 beam line and for the contribution to

the installation of the experiment. We have benefited from instructive discussions with A. Capella, H. Kühn, N. Nikolaev, and L. Stodolsky. We are grateful to B. Leupold and G. Lottspeich for running the computer programs and supervising the measuring at MPI Munich. The Liverpool authors acknowledge the financial support of the Science and Engineering Research Council.

\*On leave from R. Boskovic Institute, Zagreb, Yugoslavia.

†Permanent address: Fermilab, Batavia, Illinois.

‡Deceased.

§Visitor from the Institute of Physics and Nuclear Techniques of Academy of Mining and Metallurgy, Krakow, Poland.

<sup>1</sup>See, for example, W. Busza, *Acta Phys. Pol.* **8**, 333 (1977); A. Capella and A. Krzywicki, *Phys. Rev. D* **18**, 3357 (1978); S. Fredrikson, Report No. Ref. Th. 2720-CERN, 1979 (unpublished); A. Białas, in *Proceedings of the First Workshop on Ultra-Relativistic Nuclear Collisions, Berkeley, California, 1979* (LBL, Berkeley, 1979), p. 63; D. S. Barton, in *Proceedings of the XIth International Symposium on Multiparticle Dynamics, Bruges, Belgium, 1980*, edited by E. DeWolf and F. Verbeure (Univ. Antwerp, Antwerp, Belgium, 1980), p. 211; M. A. Fessler, *Ann. Phys.* **137**, 44 (1981); N. N. Nikolaev, *Usp. Fiz. Nauk* **134**, 369 (1981) [*Sov. Phys. Usp.*, translation to be published].

<sup>2</sup>J. Babecki and G. Nowak, *Acta Phys. Pol.* **B9**, 401 (1978).

<sup>3</sup>I. Derado, *Fizika* **13**, 85 (1981), Suppl. A; in *Proceedings of the International Conference on High Energy Physics, Lisbon, 1981* (unpublished); P. Seyboth, in *Multiparticle Dynamics 1981*, proceedings of the XII International Symposium, Notre Dame, Indiana, edited by W. D. Shephard and V. P. Kenney (World Scientific, Singapore, 1982), p. 217.

<sup>4</sup>Proposal No. CERN/SPSC/75-1/P37 (unpublished).

<sup>5</sup>G. Charlton *et al.*, *Phys. Rev. Lett.* **29**, 515 (1972).

<sup>6</sup>A. S. Carroll *et al.*, *Phys. Lett.* **80B**, 319 (1979).

<sup>7</sup>I. Dostrovsky *et al.*, *Phys. Rev.* **111**, 1659 (1958).

<sup>8</sup>Z. Koba, N. B. Nielsen, and P. Olesen, *Nucl. Phys.* **B40**, 317 (1970).

<sup>9</sup>P. Slattery, *Phys. Rev. Lett.* **29**, 1624 (1972).

<sup>10</sup>M. Jeżabek and K. Zalewski, *Acta Phys. Pol.* **B11**,

425 (1980); C. Pajares and A. V. Ramallo, *Phys. Lett.* **107B**, 238 (1981).

<sup>11</sup>J. E. Elias *et al.*, *Phys. Rev. D* **22**, 13 (1980).

<sup>12</sup>A. Wróblewski, *Acta Phys. Pol.* **B4**, 857 (1973).

<sup>13</sup>A. Białas and W. Czyż, *Phys. Lett.* **58B**, 325 (1975).

<sup>14</sup>W. Thomé *et al.*, *Nucl. Phys.* **B129**, 365 (1977).

<sup>15</sup>S. A. Azimov *et al.*, *Phys. Lett.* **73B**, 500 (1978).

<sup>16</sup>S. Uhlig *et al.*, *Nucl. Phys.* **B132**, 15 (1978).

<sup>17</sup>R. Göttgens *et al.*, *Z. Phys. C* **2**, 17 (1981).

<sup>18</sup>S. Brodsky, J. Gunion, and H. Kühn, *Phys. Rev. Lett.* **39**, 1120 (1977).

<sup>19</sup>A. Capella and J. Trân Thanh Vân, *Phys. Lett.* **93B**, 146 (1980); *Z. Phys. C* **10**, 249 (1981).

<sup>20</sup>A. Capella, in *Partons in Soft Hadronic Processes*, proceedings of the Europhysics Study Conference, Erice, 1981, edited by R. T. Van de Walle (World Scientific, Singapore, 1981), p. 199; A. Capella and J. Trân Thanh Vân (private communication).

<sup>21</sup>W. Chao *et al.*, *Phys. Rev. Lett.* **44**, 518 (1980).

<sup>22</sup>N. N. Nikolaev and A. Y. Ostapchuck, Report No. CERN Th.-2575, 1978 (unpublished).

<sup>23</sup>A. Białas, W. Czyż, and W. Furmanski, *Acta Phys. Pol.* **B8**, 585 (1977).

<sup>24</sup>V. V. Anisovich, Yu. M. Shabelsky, and V. M. Shekhter, *Nucl. Phys.* **B135**, 477 (1978).

<sup>25</sup>N. N. Nikolaev, Max-Planck-Institut für Physik Report No. MPI-PAE/PTH 41/81 (unpublished); and private communications.

<sup>26</sup>R. I. Glauber, *Lectures in Theoretical Physics* (Interscience, New York, 1959), Vol. 1. V. N. Gribov, *Zh. Eksp. Teor. Fiz.* **57**, 1306 (1969) [*Sov. Phys. JETP* **30**, 709 (1970)].

<sup>27</sup>L. D. Landau, in collected papers by D. Ter Haar, (Pergamon, New York, 1965), p. 586; L. Stodolsky, in *Proceedings of the VI International Colloquium on Multiparticle Reactions, Oxford, 1975* (Rutherford Laboratory, Chilton, England, 1975), p. 577.